

# Multi-Level Contrastive Learning for Dense Prediction Task

Qiushan Guo<sup>1</sup>, Yizhou Yu<sup>1</sup>, Yi Jiang<sup>2</sup>, Jiannan Wu<sup>1</sup>, Zehuan Yuan<sup>2</sup>, Ping Luo<sup>1</sup>  
<sup>1</sup>The University of Hong Kong <sup>2</sup>ByteDance Inc.

## Abstract

In this work, we present *Multi-Level Contrastive Learning for Dense Prediction Task (MCL)*, an efficient self-supervised method for learning region-level feature representation for dense prediction tasks. Our method is motivated by the three key factors in detection: localization, scale consistency and recognition. To explicitly encode absolute position and scale information, we propose a novel pretext task that assembles multi-scale images in a montage manner to mimic multi-object scenarios. Unlike the existing image-level self-supervised methods, our method constructs a multi-level contrastive loss that considers each sub-region of the montage image as a singleton. Our method enables the neural network to learn regional semantic representations for translation and scale consistency while reducing pre-training epochs to the same as supervised pre-training. Extensive experiments demonstrate that MCL consistently outperforms the recent state-of-the-art methods on various datasets with significant margins. In particular, MCL obtains 42.5  $AP^{bb}$  and 38.3  $AP^{mk}$  on COCO with the 1x schedule finetuning, when using Mask R-CNN with R50-FPN backbone pre-trained with 100 epochs. In comparison to MoCo, our method surpasses their performance by 4.0  $AP^{bb}$  and 3.1  $AP^{mk}$ . Furthermore, we explore the alignment between pretext task and downstream tasks. We extend our pretext task to supervised pre-training, which achieves a similar performance to self-supervised learning. This result demonstrates the importance of the alignment between pretext task and downstream tasks, indicating the potential for wider applicability of our method beyond self-supervised settings. Code will be released at <https://github.com/GuoQiushan/MCL>.

## 1. Introduction

A generic large-scale supervised pre-training is a critical auxiliary task for the computer vision community to progress, like ImageNet[16] pre-training, which has been validated by many works [18, 25, 26, 33, 41, 42, 46]. The benefits of initializing the model with pre-trained weights include faster convergence and better generality for down-

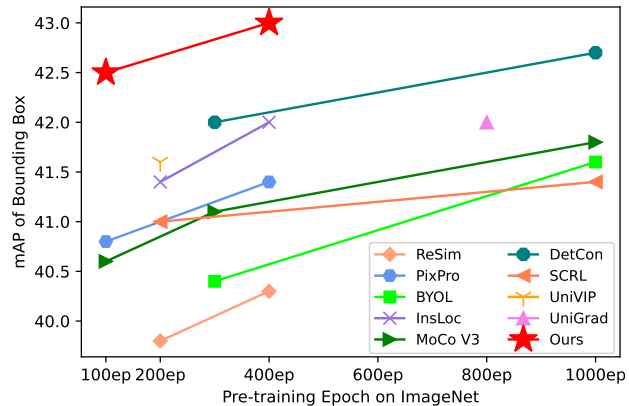


Figure 1: Our efficient self-supervised learning method, MCL, consistently outperforms the previous state-of-the-art methods on the COCO detection downstream task, while significantly reducing the pre-training epochs. MCL pre-trained on ImageNet for 100 epochs obtains 42.5  $AP^{bb}$  and 38.3  $AP^{mk}$  on COCO dataset with the standard 1x schedule [56]. Transfer performance is measured by finetuning a Mask-RCNN with ResNet50-FPN backbone.

stream tasks. Recently, self-supervised learning (SSL) based on instance discrimination tasks has driven many advances, achieving state-of-the-art results on the challenging ImageNet dataset under the  $k$ -NN and linear probing evaluation policy. Despite their advanced performance on classification tasks, some recent works [39, 53, 54, 60, 62] have pointed out a common weakness of these methods: The image-level representation learning does not transfer well to dense prediction tasks, such as object detection and instance segmentation. Additionally, the success of state-of-the-art methods [7, 10, 22, 24, 28] requires several times more training epochs than supervised pre-training.

In contrast to the ImageNet classification task, where objects have a small variation in scale, object detection datasets typically have a large scale variation across object instances, and precise localization of objects is required. Therefore, an ideal detector is supposed to be scale-consistent across object instances and encode position information accurately. Pixel-level SSL methods [35, 53] consider the spatial structure information as shown in Fig. 2(a). These pretext tasks treat each pixel in an image as a single instance and encourage the model to distinguish each pixel

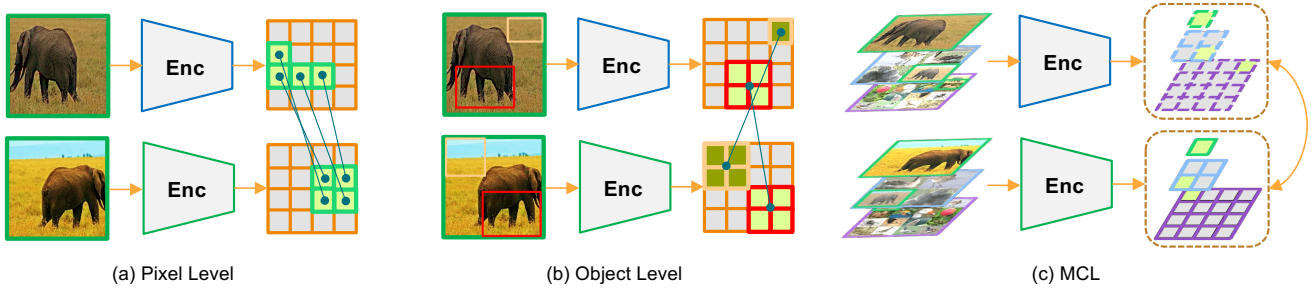


Figure 2: (a) Pixel-level methods match positive feature pairs based on the transportation cost of feature distance, which does not guarantee precise assignment. (b) Object-level methods obtain localization by off-the-shelf algorithms, whose predictions are low-quality on a non-object-centric dataset. (c) Our method assembles multiple augmented views with different sizes in a montage manner and constructs multi-level contrastive learning on each sub-image. As a result, MCL learns regional representation for precise localization, scale consistency among multi-scale crops and semantic representation that generalizes well on the dense prediction tasks.

from others within the image. Unfortunately, the matching rule of positive pixel pair is based on the transportation cost of feature distance, which does not guarantee precise and stable feature target assignment. Object-level SSL methods [28, 54] focus on the proposals from some off-the-shelf algorithms, such as Selective Search [51] and Multi-scale Combinatorial Grouping [4], as illustrated in Fig. 2(b). However, the bounding box and segmentation mask proposals are not accurate enough on the non-object-centric dataset, such as COCO. The low-quality proposals yield an inferior result for the downstream dense prediction tasks due to the localization noise.

Our proposed method, Multi-Level Contrastive Learning (MCL), is motivated by the key factors of detection: localization, scale consistency, and recognition. MCL is a novel and highly efficient self-supervised learning framework for dense prediction tasks, which has achieved state-of-the-art transfer performance on downstream tasks while significantly reducing the training epochs. To achieve localization, scale consistency, and recognition, we design a montage assembly that assembles multi-scale images into a non-overlapping grid, mimicking multi-object scenarios. The montage assembly explicitly encodes the position and scale information of images. Additionally, we adopt a scale-aware positive target assignment strategy on the feature pyramid, which produces a multi-scale feature representation with strong semantic information. Moreover, MCL proposes a series of contrastive modes to improve scale consistency. Each component image in the montage image is treated as an independent instance, and features are accurately extracted based on image coordinates. This bridging of the gap between the pretext task and downstream tasks ensures accurate feature target assignment. To further investigate the alignment between pretext task and downstream tasks, we extend our pretext task to supervised pre-training. Our supervised pre-training achieves similar performance to self-supervised pre-training, demonstrating the importance of task alignment.

To evaluate MCL, we conduct extensive experiments on benchmarks for various dense prediction tasks. As shown in Fig. 1, MCL achieves state-of-the-art transfer performance pretrained on the ImageNet dataset, while significantly reducing the training cost to 100 epochs on ImageNet. MCL pre-trained on ImageNet for 100 epochs obtains 42.5  $AP^{bb}$  and 38.3  $AP^{mk}$  on the COCO dataset with the standard 1x schedule [56] and surpasses MoCo by 4.0  $AP^{bb}$  and 3.1  $AP^{mk}$ , using Mask R-CNN with R50-FPN backbone. MCL pre-trained on the unlabeled COCO dataset also achieves a state-of-the-art result, 41.8  $AP^{bb}$  and 37.7  $AP^{mk}$ . This result shows that MCL benefits from the carefully designed multi-level pretext task rather than the dataset bias [40].

Our contributions are listed as follows: (1) An efficient self-supervised method, Multi-level Contrastive Learning, is designed to align the pretext task with the dense prediction tasks, improving scale invariance and localization precision. (2) Montage assembly is introduced in the self-supervised learning field for **the first time** to construct a montage image, mimicking multi-scale multi-object scenarios. (3) Our method achieves **state-of-the-art** transfer performance on the dense prediction downstream tasks, such as detection, segmentation, and pose estimation while reducing the pre-training cost to 100 ImageNet epochs.

## 2. Related Work

**Instance contrastive learning.** Instance-level contrastive learning considers each image as a singleton, only one sample in a class [6], which considers two augmented views of the same image as positive to be pulled closer, and all other images negative to be pushed further apart. MemoryBank [57] stores previously-computed representation in a memory bank to compare instances based on noise contrastive estimation. MoCo [24] uses a momentum encoder to store representation in a temporal manner, allowing the dictionary to be large. SimCLR [10, 11] shows that the memory bank is not necessary when the mini-batch size is large enough. SwAV [7] clusters the data while enforcing consistency between cluster assignments. Besides,

SwAV adopts multi-crop data augmentation, which uses a mix of views with different resolutions in place of two full-resolution views. BYOL [22] and SimSiam [10] explore directly maximizing the similarity between two views of one image without negative pairs. Despite the success of instance-level contrastive learning on ImageNet linear probing, instance-wise contrastive learning does not encode position information explicitly, treating all regions equally. In contrast, MCL views each subimage in the montage image as a singleton to explicitly encode image localization with high fidelity.

**Dense Representation Learning.** Dense representation learning predicts at the pixel level, compared with the instance contrastive learning. Recently, some self-supervised learning methods that learn at pixel level representation are proposed. UL DVR [39] learns pixel-wise representation by forcing local features to remain constant over different view conditions. DCL [53] optimizes a pairwise contrastive similarity loss at the pixel level between two views of input images by the Hungarian matching strategy. Self-EMD [35] shares a similar basic idea, but updates the matching strategy to Earth Mover’s distance [44]. PixPro [60] matches the feature pixels by a hand-crafted decision rule. These matching strategies only implicitly map the localization in feature maps to the euclidean coordinate in the input image, but do not guarantee a precise feature target assignment. Different from the pixel-level label assignment, MCL assigns a positive sample by matching the image regions with different sizes in the montage image on multi-level feature maps. Our scale-aware assignment strategy ensures the precision localization of each feature point.

**Object-Level Representation Learning.** Both single-stage detectors and two-stage detectors attend to a manageable number of candidate object regions and evaluate convolutional networks on each region. The regions of interest have rectangular shapes and come in different sizes. RoIAlign [26] is proposed to extract the features of particular regions on the convolutional feature maps. Following Fast-RCNN [21], SoCo [54] selects the proposal bounding boxes generated from Selective Search [51] and applies RoIAlign to extract object features by constructing multiple augmented views, which is used for contrastive loss. DetCon [28] identifies object-based regions with the off-the-shelf approximate segmentation algorithms [4, 19] to produce a semantic mask. The contrastive detection objective then pulls together pooled feature vectors from the same mask and pushes apart features from different masks and different images. Whereas, the segmentation mask and bounding box predicted by the off-the-shelf methods are not accurate enough, incurring pseudo-label noise, which leads to an inferior result on the non-object-centric dataset. In contrast, MCL constructs montage images and precisely annotates the localization of each component image. As a

result, MCL maintains a high transfer performance when pre-trained on the COCO dataset.

### 3. Method

Our goal is to learn regional semantic representation and scale consistency without supervision while keeping the training epoch reasonable. While instance-level SSL methods [24, 37] have shown success in learning occlusion-invariant representations [40], we present a new approach that applies instance discrimination at the region level for learning visual representations that generalize well to dense prediction tasks. As illustrated in Fig. 3, our method, MCL, constructs multiple augmented views in different sizes and produces a multi-scale feature pyramid, on which a contrastive loss is applied across the levels. The montage assembly guarantees the precision of pseudo bounding box label, which explicitly encodes the absolute position information. To align the pretext task and downstream tasks, all the network modules in the downstream model are pre-trained for a well-initialized representation. We also extend our pretext task to supervised pre-training and provide more details on this in Appendix.

---

#### Algorithm 1 Montage Pseudo Code

---

```
# s: the level of downsampling ratio
# x: the input images batch with shape of (B, C, H, W)
ratio = pow(2, s)
x_aug = aug(x) # data augmentation
x_aug_ds = interpolate(x_aug, scale_factor = 1. / ratio)
x_aug_ds = shuffle(x_aug_ds)
B_ds = B / ratio / ratio
H_ds, W_ds = H / ratio, W / ratio
x_aug_ds = x_aug_ds.reshape(B_ds, ratio, ratio, C, H_ds, W_ds)
x_aug_ds = x_aug_ds.permute(0, 3, 1, 4, 2, 5)
x_aug_ds = x_aug_ds.reshape(B, C, H, W)
```

---

#### 3.1. Montage Assembly

The photomontage is the process and the result of making a composite photograph by cutting, gluing, rearranging, and overlapping two or more photographs into a new image. An interesting observation is that montage process assembles images in different scales at specific locations, which explicitly encodes the position and scale information. In our approach, the image batch  $X$  is processed through the same augmentation pipeline with different random seeds. To handle the large scale variation, the augmented images are downsampled to  $\frac{1}{2^s}$  of the original size, where the  $s$  ranges from  $\{0, 1, 2, \dots, S - 1\}$  and matches the level of feature maps in FPN. To encode position and scale information, all the downsampled images with the same downsampling ratio are randomly combined to construct a montage image. The resulting montage images have aligned shapes with the original augmented images. The pseudo code for this process is provided in Alg. 1 for clarity.

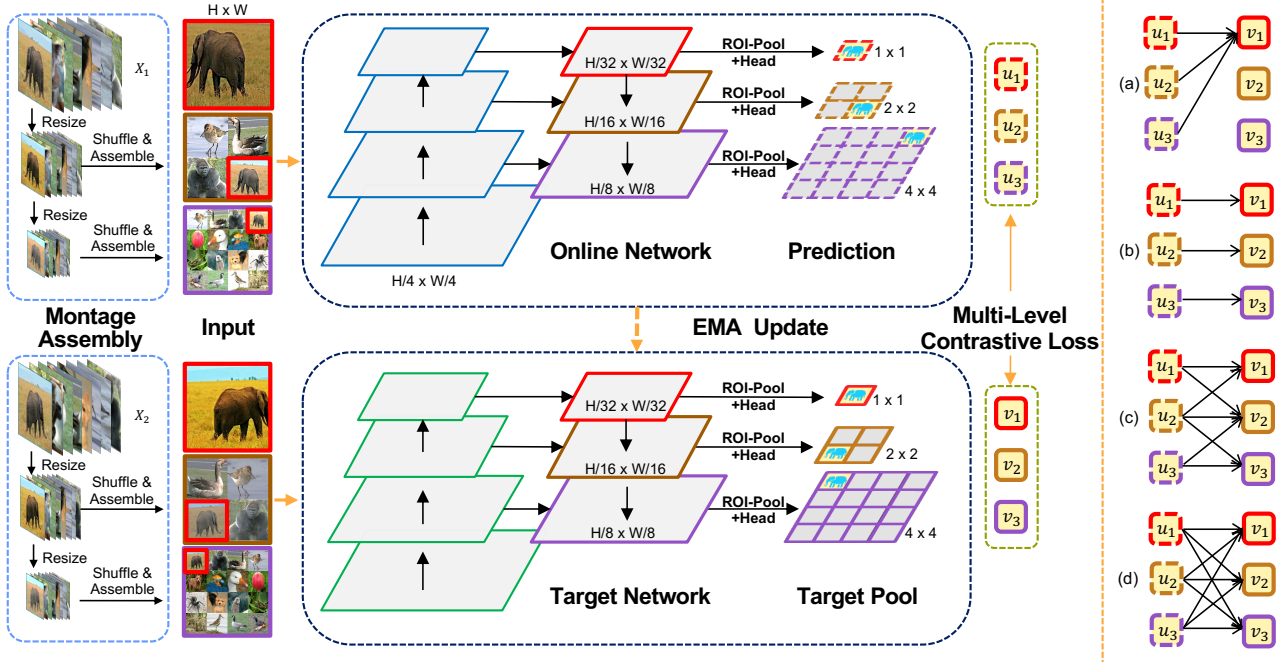


Figure 3: Overview of our method. This figure illustrates MCL with a model, whose FPN contains 3 levels. The image batch  $X$  is processed via the same augmentation pipeline with different random seeds. The images are downsampled by a factor of 2 and shuffled to construct montage input. The subfigures are multi-scale and precisely localized. The feature pyramid is further ROI-pooled according to the subfigure location. Contrastive learning is performed on multi-level features to learn semantic regional representations via scale consistency regularization.  $u_i$  and  $v_i$  are extracted from the  $i$ -th level feature pyramid. The arrow means to set the corresponding target feature as the positive sample and the other target features at the same level as the negative samples. The target network is not optimized by gradient and updated by the online network in an EMA manner.

### 3.2. Multi-Level Contrastive Learning

Detectors with FPN assign anchor boxes of scale within a range to a specific pyramid level. Following this basic idea, we propose to extract features from FPN according to the downsampling ratio. Concretely, we assign the images with a downsampling ratio of  $2^s$  to  $P_{5-s}$  for a 3-level FPN architecture, where we denote the final feature set of FPN as  $\{P_3, P_4, P_5\}$  from the finest resolution map to the coarsest resolution map. Similar to the RoI pooling operator, we map the rectangular window of the component images onto the FPN features and aggregate the features using a global average pooling layer. Subsequently, the dense prediction head processes the features. For the non-FPN framework, we construct a feature pyramid by interpolating the final feature map to the specific sizes.

To encode the augmented views, we use two encoders: the online network  $f_\theta$  and the target network  $f_{\theta'}$ . The target network is implemented as an exponential moving average (EMA) of the online network. The online network is appended with a projector  $g_\theta$  and a predictor  $h_\theta$ , while the target network only has a projector  $g_{\theta'}$ . We represent each view pair as normalized latent features  $\mathbf{u}_{s_i}$  and  $\mathbf{v}_{s_i}$ , where  $\mathbf{I}_{s_i}$  is the image assembled by the subimages whose downsampling ratio is  $s_i$ ,

$$\mathbf{u}_{s_i} = h_\theta \circ g_\theta \circ f_\theta(\mathbf{I}_{s_i}), \quad \mathbf{v}_{s_i} = g_{\theta'} \circ f_{\theta'}(\mathbf{I}'_{s_i}). \quad (1)$$

We adopt the contrastive loss function in the form of InfoNCE [52] to optimize the model:

$$\mathcal{L}_u = -\log \frac{\exp(\mathbf{u} \cdot \mathbf{v}^+ / \tau)}{\exp(\mathbf{u} \cdot \mathbf{v}^+ / \tau) + \sum_{\mathbf{v}^-} \exp(\mathbf{u} \cdot \mathbf{v}^- / \tau)}, \quad (2)$$

where the subscript of latents are omitted for simplicity. Here,  $\mathbf{v}^+$  is the target network's output on the same subimage as  $\mathbf{u}$  and the set  $\{\mathbf{v}^-\}$  is composed of target network's outputs from other subimages.  $\tau$  is a temperature hyperparameter [50] for  $l_2$ -normalized latent features. Note that, the feature maps  $\mathbf{u}_{s_i}$  and  $\mathbf{v}_{s_i}$  are split into vectors based on the coordinates of the subimages. As the number of latent features is sufficiently large, we use the negative samples co-existing in the same batch, following [5, 10, 29, 63]. Besides, we adopt a symmetric loss [7, 13, 22]:  $\mathcal{L} = \mathcal{L}_u + \mathcal{L}_v$ .

### 3.3. Multi-Level Contrastive Loss

To improve the scale consistency, we propose a series of modes to construct the final loss. Specifically, we design four matching strategies for assigning both the positive and the negative samples to the online features. As shown in the right part of Fig. 3, (a) All the images in different sizes target the view in the largest shape, (b) Each image level aims to pull close features from the counterpart level, (c) Latent features match the features from the adjacent levels, and (d)

Methods	AP <sup>bb</sup>	AP <sub>50</sub> <sup>bb</sup>	AP <sub>75</sub> <sup>bb</sup>	AP <sup>mk</sup>	AP <sub>50</sub> <sup>mk</sup>	AP <sub>75</sub> <sup>mk</sup>
Supervised	38.9	59.6	42.7	35.4	56.5	38.1
BYOL [22]	39.3	59.0	42.8	-	-	-
DenseCL [53]	39.8	59.7	43.3	35.8	56.6	38.6
Self-EMD [35]	40.4	61.1	43.7	-	-	-
SoCo [54]	40.6	61.1	44.4	36.4	58.1	38.1
<b>MCL</b>	<b>41.8</b>	<b>62.1</b>	<b>45.8</b>	<b>37.7</b>	<b>59.3</b>	<b>40.5</b>

Table 1: Comparison with state-of-the-art methods on COCO *val* set. All the models are **pre-trained on COCO dataset** and fine-tuned with Mask-RCNN following 1x schedule [56].

A dense connection is applied to all levels, treating all image resolution equally. The empirical study and comparison are provided in Sec.4.3.

## 4. Experiments

In this section, we conduct a comprehensive set of experiments to evaluate our pre-training mechanism on dense prediction tasks, *e.g.*, COCO [34] detection, instance segmentation, pose estimation, Cityscapes segmentation [15] and LVIS [23] long tail object detection and segmentation.

### 4.1. Pre-training Setup

We pre-train our MCL model on ImageNet-1K [16] and COCO [34] dataset with LARS [64] optimizer and a batch size of 4096. By default, all the models are pre-trained for 100 epochs on the ImageNet training set, which contains approximately 1.28 million images. The training cost is comparable to supervised pre-training. For pre-training on the non-object-centric dataset, models are optimized for 530 epochs on the COCO training set and unlabeled set (about 241 thousand images) to match the training iteration on ImageNet. We employ the same data augmentation pipeline of BYOL [22], which is composed of random crop augmentation, random horizontal flip, color distortion, Gaussian blur, grayscaling and the solarization operation. All the component images are augmented separately with different random seeds but share an augmentation pipeline. The learning rate is linearly warmed up at the first 10 epochs and cosine annealed during the remaining epochs. The learning rate is set based on the batch size:  $lr = 1.0 \times BatchSize / 256$  and the weight decay is set to  $1e^{-5}$ . The weights of the target network are updated with a momentum coefficient  $m$ , starting from 0.99 and increased to 1 in the cosine scheduler same as [14, 22].

### 4.2. Results on Downstream Tasks

**Pre-training on Non-object-centric Dataset.** ImageNet is an object-centric dataset, which introduces dataset biases into pre-training and costs more effort to collect than non-iconic images. As indicated in Tab. 1, MCL still obtains a large improvement, 1.4 AP<sup>bb</sup>/1.3 AP<sup>mk</sup> over SoCo [54]. This result demonstrates that MCL is robust to dataset and benefits mainly from the scale-invariance and precise

Methods	Epoch	AP <sup>bb</sup>	AP <sub>50</sub> <sup>bb</sup>	AP <sub>75</sub> <sup>bb</sup>
Rand Init	-	24.5	39.0	25.7
Supervised	90	37.4	56.5	39.7
InsDis [57]	200	35.5 <sup>(-1.9)</sup>	54.1 <sup>(-2.4)</sup>	38.2 <sup>(-1.5)</sup>
PIRL [37]	200	35.7 <sup>(-1.7)</sup>	54.2 <sup>(-2.3)</sup>	38.4 <sup>(-1.3)</sup>
MoCo [24]	200	36.3 <sup>(-1.1)</sup>	55.0 <sup>(+1.5)</sup>	39.0 <sup>(-0.7)</sup>
MoCo v2 [24]	200	37.2 <sup>(+0.2)</sup>	56.2 <sup>(+0.3)</sup>	39.6 <sup>(+0.1)</sup>
InfoMin [48]	200	38.1 <sup>(+0.7)</sup>	57.3 <sup>(+0.8)</sup>	40.9 <sup>(+1.2)</sup>
SwAV [7]	400	36.5 <sup>(-0.9)</sup>	56.4 <sup>(+0.1)</sup>	38.8 <sup>(-0.9)</sup>
PixPro [60]	100	37.9 <sup>(+0.5)</sup>	56.7 <sup>(+0.2)</sup>	40.5 <sup>(+0.8)</sup>
SoCo [54]	100	38.2 <sup>(+0.8)</sup>	57.4 <sup>(+0.9)</sup>	40.9 <sup>(+1.2)</sup>
InsLoc [62]	200	36.4 <sup>(-1.0)</sup>	55.3 <sup>(-1.2)</sup>	39.0 <sup>(-0.7)</sup>
DenseCL [53]	200	37.6 <sup>(+0.2)</sup>	56.3 <sup>(+0.2)</sup>	40.3 <sup>(+0.6)</sup>
<b>MCL</b>	100	<b>39.1<sup>(+1.7)</sup></b>	<b>58.5<sup>(+2.0)</sup></b>	<b>41.8<sup>(+2.1)</sup></b>

Table 2: Results on COCO for RetinaNet. All the models are **pre-trained on ImageNet** and finetuned on COCO with 1x schedule [56]. MCL outperforms all the other state-of-the-art methods.

localization representation rather than the dataset bias. Besides, the results manifest that pixel-level SSL methods and object-level methods fail in the non-iconic scenario.

#### COCO Object Detection and Instance Segmentation.

Object detection and instance segmentation require simultaneous object location and classification while handling large variance of object size. We adopt Mask-RCNN [26] and RetinaNet [33] with ResNet-50 FPN backbone as detectors to evaluate the models pre-trained on ImageNet and COCO dataset. As shown in Tab. 3, MCL outperforms the state-of-the-art (SOTA) unsupervised pre-training methods on the COCO 1x and 2x schedules with only 100 training epochs, achieving 42.5 AP<sup>bb</sup>/38.2 AP<sup>mk</sup> and 43.4 AP<sup>bb</sup>/39.1 AP<sup>mk</sup> on the 1x and 2x schedule, respectively. Our method surpasses the supervised counterpart by 3.6 AP<sup>bb</sup> and 2.8 AP<sup>mk</sup> on 1x schedule, showing that MCL accelerates the model converging on the downstream tasks.

*To verify the extendability of MCL, we conduct experiments on RetinaNet [33], which is different from the pre-training architecture. We follow the standard COCO 1x schedule and include SyncBN in the backbone and FPN for a fair comparison. Tab. 2 shows that MCL exceeds the supervised baseline by 1.7 AP<sup>bb</sup>.*

**Finetune in a Low Data Regime.** One of the purposes of pre-training is to improve the target task performance in a low data regime. Therefore, we conduct experiments on a mini version of the COCO dataset. Specifically, we randomly sample 1, 2, 5 and 10% of COCO training data as the labeled dataset. To avoid overfitting, we finetune the detectors with 12k iterations. Other settings are the same as COCO 1x schedule. Tab. 4 indicates that MCL has strong generalization than other methods and outperforms the supervised counterparts by about 4 AP. This result shows that MCL can be extended to semi-supervised learning for ob-

Methods	Epoch	1× Schedule						2× Schedule					
		AP <sup>bb</sup>	AP <sub>50</sub> <sup>bb</sup>	AP <sub>75</sub> <sup>bb</sup>	AP <sup>mk</sup>	AP <sub>50</sub> <sup>mk</sup>	AP <sub>75</sub> <sup>mk</sup>	AP <sup>bb</sup>	AP <sub>50</sub> <sup>bb</sup>	AP <sub>75</sub> <sup>bb</sup>	AP <sup>mk</sup>	AP <sub>50</sub> <sup>mk</sup>	AP <sub>75</sub> <sup>mk</sup>
Rand Init	-	31.0	49.5	33.2	28.5	46.8	30.4	38.4	57.5	42.0	34.7	54.8	37.2
Supervised	90	38.9	59.6	42.7	35.4	56.5	38.1	41.3	61.3	45.0	37.3	58.3	40.3
Bringing[1]	100	36.5	-	-	33.6	-	-	-	-	-	-	-	-
MoCo [24]	200	38.5	58.9	42.0	35.1	55.9	37.7	40.8	61.6	44.7	36.9	58.4	39.7
MoCo v2 [12]	200	40.4	60.2	44.2	36.4	57.2	38.9	41.7	61.6	45.6	37.6	58.7	40.5
MoCo v3 [14]	300	41.1	61.6	45.0	37.3	58.8	40.0	-	-	-	-	-	-
InfoMin [48]	200	40.6	60.6	44.6	36.7	57.7	39.4	42.5	62.7	46.8	38.4	59.7	41.4
UniVIP [32]	200	41.6	-	-	37.6	-	-	43.1	-	-	38.8	-	-
BYOL [22]	300	40.4	61.6	44.1	37.2	58.8	39.8	42.3	62.6	46.2	38.3	59.6	41.1
SwAV [7]	400	41.2	62.1	45.0	37.3	59.0	40.2	42.3	62.8	46.3	38.2	60.0	41.0
VICRegL[2]	400	37.3	-	-	34.1	-	-	-	-	-	-	-	-
DINO [8]	800	41.2	-	-	37.1	-	-	42.3	-	-	38.1	-	-
UniGrad [47]	800	42.0	62.6	45.7	37.9	59.7	40.7	-	-	-	-	-	-
SparK [3]	1600	41.6	-	-	37.7	-	-	-	-	-	-	-	-
PLRC[38]	100	39.3	58.8	43.1	35.5	55.9	37.9	-	-	-	-	-	-
DCL [53]	200	40.3	59.9	44.3	36.4	57.0	39.2	41.2	61.9	45.1	37.3	58.9	40.1
ReSim [58]	200	39.8	60.2	43.5	36.0	57.1	38.6	41.4	61.9	45.4	37.5	59.1	40.3
RCL [61]	200	40.4	61.3	44.2	36.7	58.2	39.4	42.1	62.9	45.9	38.0	60.0	40.7
DetCon [28]	300	42.0	-	-	37.8	-	-	-	-	-	-	-	-
PixPro [60]	400	41.4	61.6	45.4	-	-	-	-	-	-	-	-	-
InsLoc [62]	400	42.0	62.3	45.8	37.6	59.0	40.5	43.3	63.6	47.3	38.8	60.9	41.7
SCRL [43]	800	41.3	62.4	45.0	37.7	59.6	40.7	-	-	-	-	-	-
MCL	100	42.5	62.8	46.9	38.2	59.8	41.2	43.4	63.6	47.5	39.1	60.8	41.9
<b>MCL</b>	<b>400</b>	<b>43.0</b>	<b>63.3</b>	<b>47.4</b>	<b>38.6</b>	<b>60.2</b>	<b>41.7</b>	<b>44.0</b>	<b>64.2</b>	<b>48.3</b>	<b>39.5</b>	<b>61.3</b>	<b>42.7</b>

Table 3: Comparison with SOTA methods on COCO by using Mask R-CNN. All the detectors are evaluated on COCO *val* 2017 set. “-” means that the results are missing in the source paper. MCL outperforms all the other SOTA SSL methods while significantly reducing the training epochs.

Methods	1% Data			2% Data			5% Data			10% Data		
	AP	AP <sub>50</sub>	AP <sub>75</sub>									
Rand Init	1.4	3.5	1.0	2.5	5.6	2.0	3.6	7.4	3.0	3.7	7.5	3.2
Supervised	8.2	16.2	7.2	11.2	21.7	10.3	16.5	30.3	15.9	19.6	34.5	19.7
MoCo[24]	7.0 <sup>(-1.2)</sup>	13.5 <sup>(-2.7)</sup>	6.5 <sup>(-0.7)</sup>	10.3 <sup>(-0.9)</sup>	19.2 <sup>(-2.5)</sup>	9.7 <sup>(-0.6)</sup>	15.0 <sup>(-1.5)</sup>	27.0 <sup>(-3.3)</sup>	14.9 <sup>(-1.0)</sup>	18.2 <sup>(-1.4)</sup>	31.6 <sup>(-2.9)</sup>	18.4 <sup>(-1.3)</sup>
MoCo v2[12]	8.4 <sup>(+0.2)</sup>	15.8 <sup>(+0.4)</sup>	8.0 <sup>(+0.8)</sup>	12.0 <sup>(+0.8)</sup>	21.8 <sup>(+0.1)</sup>	11.5 <sup>(+1.2)</sup>	16.8 <sup>(+0.3)</sup>	29.6 <sup>(+0.7)</sup>	16.8 <sup>(+0.9)</sup>	20.0 <sup>(+0.4)</sup>	34.3 <sup>(+0.2)</sup>	20.2 <sup>(+0.5)</sup>
DetCo[59]	9.9 <sup>(+1.7)</sup>	19.3 <sup>(+3.1)</sup>	9.1 <sup>(+1.9)</sup>	13.5 <sup>(+2.3)</sup>	25.1 <sup>(+3.4)</sup>	12.7 <sup>(+2.4)</sup>	18.7 <sup>(+2.2)</sup>	32.9 <sup>(+2.6)</sup>	18.7 <sup>(+2.8)</sup>	21.9 <sup>(+2.3)</sup>	37.6 <sup>(+3.1)</sup>	22.3 <sup>(+2.6)</sup>
<b>MCL</b>	<b>12.1<sup>(+3.9)</sup></b>	<b>22.6<sup>(+6.4)</sup></b>	<b>11.6<sup>(+4.4)</sup></b>	<b>15.4<sup>(+4.2)</sup></b>	<b>27.0<sup>(+5.3)</sup></b>	<b>15.6<sup>(+5.3)</sup></b>	<b>20.7<sup>(+4.2)</sup></b>	<b>35.5<sup>(+5.2)</sup></b>	<b>20.7<sup>(+4.8)</sup></b>	<b>23.8<sup>(+4.2)</sup></b>	<b>39.6<sup>(+5.1)</sup></b>	<b>24.2<sup>(+4.5)</sup></b>

Table 4: Results of finetuning model in a low data regime. One-stage detection fine-tuned on COCO 1%, 2%, 5% and 10% data. All methods **except** MCL are pre-trained 200 epochs on ImageNet. MCL is pre-trained for 100 epochs.

ject detection as a consistency regularization.

**Finetune on LVIS Dataset.** Compared with COCO, LVIS v1 dataset [23] is more challenging due to the long tail distribution, which contains 1203 categories. To demonstrate the effectiveness and generality of our method, we finetune a Mask R-CNN model and follow the standard LVIS v1 1x training schedule. Tab. 5 shows that MCL significantly improves the performance on rare categories by 4.3 AP<sup>bb</sup>/4.3 AP<sup>mk</sup>, which is much larger than the improvement on the common and frequent categories.

**ADE20K, Cityscapes and COCO KeyPoint Dataset.** To evaluate our method on other downstream tasks, we choose ADE20K, Cityscapes and COCO KeyPoint dataset. We evaluate MCL with Mask R-CNN and Semantic FPN

on Cityscapes dataset, with UperNet on ADE20K-847 datasets. For the COCO Keypoint dataset, we attach the standard keypoint head on Mask R-CNN. As shown in Tab. 6 and Tab. 9, MCL achieves 35.7 AP<sup>mk</sup> on Cityscapes instance segmentation task, 76.1 mIoU on the semantic segmentation task and 66.8 AP<sup>kp</sup> on COCO Keypoint task. The superior results show that MCL is suitable for dense prediction tasks besides the detection task.

**Supervised Pre-training on Transformer and CNN with MCL Pretext Task.** It seems like a foregone conclusion that self-supervised pre-training surpasses the supervised counterpart on downstream tasks. However, we find that MCL pretext task facilitates the finetuning of supervised pre-training. For a fair comparison, we pre-train mod-

Methods	AP <sup>bb</sup>	AP <sup>bb</sup> <sub>r</sub>	AP <sup>bc</sup>	AP <sup>bb</sup> <sub>f</sub>	AP <sup>mk</sup>	AP <sup>mk</sup> <sub>r</sub>	AP <sup>mk</sup> <sub>c</sub>	AP <sup>mk</sup> <sub>f</sub>
Supervised	23.9	10.2	21.8	32.2	23.1	11.1	21.6	30.1
<b>MCL</b>	<b>26.2</b>	<b>14.5</b>	<b>23.4</b>	<b>34.0</b>	<b>25.5</b>	<b>15.4</b>	<b>23.9</b>	<b>31.6</b>

Table 5: Transfer Learning on LVIS dataset using Mask R-CNN with R50-FPN trained for 180k iterations. MCL significantly improves the performance on **rare** categories by 4.3 AP<sup>bb</sup>/4.3 AP<sup>mk</sup>.

Methods	AP <sup>bb</sup>	AP <sup>bb</sup> <sub>50</sub>	AP <sup>bb</sup> <sub>75</sub>	AP <sup>kp</sup>	AP <sup>kp</sup> <sub>50</sub>	AP <sup>kp</sup> <sub>75</sub>
Supervised	57.5	84.0	63.0	65.6	87.0	71.3
<b>MCL</b>	<b>58.9</b> <sup>(+1.4)</sup>	<b>85.2</b> <sup>(+1.2)</sup>	<b>65.1</b> <sup>(+2.1)</sup>	<b>66.8</b> <sup>(+1.2)</sup>	<b>87.8</b> <sup>(+0.8)</sup>	<b>72.8</b> <sup>(+1.5)</sup>

Table 6: Results of Mask R-CNN on COCO Keypoint dataset. The results demonstrate that MCL is available for other dense prediction task besides detection task.

Methods	ResNet-50		Swin-T	
	AP <sup>bb</sup>	AP <sup>mk</sup>	AP <sup>bb</sup>	AP <sup>mk</sup>
Vanilla	38.9	35.4	43.9	39.6
<b>MCL</b>	<b>42.1</b>	<b>37.8</b>	<b>44.7</b>	<b>40.3</b>

Table 7: Supervised pre-training results. Models are pre-trained with the same data augmentation as standard supervised pre-training (Vanilla).

Methods	Sup	Sup + Mosaic	SSL + Mosaic	SSL + Copy-Paste	<b>MCL</b>
AP <sup>bb</sup>	38.9	40.1	41.1	42.0	<b>43.0</b>
AP <sup>mk</sup>	35.4	36.3	37.2	37.6	<b>38.6</b>

Table 8: Results of Mask-RCNN under 1x schedule on COCO val set. We conduct experiments with Mosaic and Copy-Paste data augmentation under both supervised and self-supervised pre-training settings. The results demonstrate that MCL outperform the other methods.

Methods	Cityscapes			ADE20k-847
	mIoU	AP <sup>mk</sup>	AP <sup>mk</sup> <sub>50</sub>	mIoU
Supervised	72.9	31.8	58.5	17.2
<b>MCL</b>	<b>76.1</b>	<b>35.7</b>	<b>63.9</b>	<b>20.8</b>

Table 9: Results of Mask R-CNN and Semantic FPN on Cityscapes dataset. Results of UperNet on ADE20K-847 datasets.

els with the same epochs as the normal supervised learning. Concretely, ResNet-50 [27] is trained with 100 epochs and Swin-T [36] is trained with 300 epochs. The other hyperparameters keep unchanged. The evaluation is still based on COCO 1x training schedule. Mask R-CNN with Swin-T is finetuned with MMDetection [9]. Tab. 7 shows that MCL outperforms 3.2 AP<sup>bb</sup>/2.4 AP<sup>mk</sup> over supervised counterpart for ResNet-50 and the unsupervised counterpart as shown in Tab. 3. The results demonstrate that *MCL pretext task is effective for the Transformer architecture with attention module*, surpassing the baseline by 0.8 AP<sup>bb</sup>/0.7 AP<sup>mk</sup>.

**Comparison with other augmentation.** Mosaic [65] and Copy-Paste [20] are similar to MCL. Compared with these methods, MCL contains sub-images in multi-sizes, which improves scale consistency, and targets the view in the largest resolution, learning more semantic information. As shown in Tab. 8, MCL outperforms supervised and self-supervised Mosaic pre-training.

### 4.3. Ablation Study

**Montage Level.** Our method is based on montage assembly over the multi-level downsampled images and contrastive learning. We investigate the effect of the montage level by pretraining models with different downsampling levels. By comparing the penultimate and the last line in Tab. 10a, the results show that the representation of fine-grained objects, whose size is less than  $28 \times 28$  pixels, is important for the object detector. This phenomenon demonstrates that the alignment of instance scale range is important between the pre-training dataset and the target dataset and that object detectors benefit from our multi-level scale consistency contrastive learning.

**Multi-Level Contrastive Loss.** As shown in Fig. 3, we propose a series of meaningful positive pair matching strategies. The loss indicators in Tab. 10b are the same as those in Fig. 3. We find that setting the images with the largest resolution as positive pair samples leads to the best result.

This result is reasonable because a higher resolution typically yields a better representation. The reason why *b* loss mode is inferior can be that the supervision from the counterpart level lacks semantic information for the small component images. The result of *c* loss mode is slightly better than *b* mode due to the feature matching across levels. The cause of *d* loss mode yielding a lower result than *c* is probably that the representation from the low-resolution image is inferior to that from the high-resolution image.

**Boundary smoothness.** The boundary of the subimages is a sudden appearance change, which may be problematic for self-supervised representation learning. To verify if the boundary is problematic, we smooth the boundary with a Gaussian mask. The standard deviation of the mask ( $\sigma_x, \sigma_y$ ) is set to  $(k \times W, k \times H)$ , where  $k$  is set to 0.5 or 0.75,  $H$  is the height of the subimage and  $W$  is the width of the subimage. The Gaussian mask softens the boundary gap and highlights the center. As indicated in Tab. 10c, assembling the origin subimages directly yields the best result. We believe that the Average RoI-pooling alleviates the boundary issue and the Gaussian mask may cause the information loss of some objects located at the boundary.

**Weight Decay.** Weight norm is an important factor in the alignment between pre-training and finetuning. We empirically demonstrate this by modifying the weight decay, which influences the weight norm of the converged model. Typically, the weight decay is set to  $1e^{-6}$  for LARS optimizer, which is widely adopted in unsupervised pre-training works [7, 10, 14, 22]. We set the weight decay from  $1.5e^{-6}$  to  $1e^{-5}$  to evaluate the effect. The results in Tab. 10d show that a large weight decay leads to a superior result. Additionally, we divide the non-normalization layer parameters by a fixed number to downscale the weight norm. The results show that reducing the weight norm of a model pre-trained with a small weight decay leads to a non-negligible improvement. Normalization techniques exist in many mainstream models [17, 27, 30, 36, 49, 45, 55],

Level	AP <sup>bb</sup>	AP <sup>bb</sup> <sub>50</sub>	AP <sup>bb</sup> <sub>75</sub>	AP <sup>mk</sup>	AP <sup>mk</sup> <sub>50</sub>	AP <sup>mk</sup> <sub>75</sub>
1	40.7	60.9	44.6	36.8	58.0	39.8
2	41.4	61.6	45.4	37.3	58.6	39.9
3	41.8	61.7	45.5	37.6	58.8	40.2
4	42.5	62.8	46.9	38.2	59.8	41.2

(a) Study on Downsampling Level.

Loss	AP <sup>bb</sup>	AP <sup>bb</sup> <sub>50</sub>	AP <sup>bb</sup> <sub>75</sub>	AP <sup>mk</sup>	AP <sup>mk</sup> <sub>50</sub>	AP <sup>mk</sup> <sub>75</sub>
a	42.5	62.8	46.9	38.2	59.8	41.2
b	41.8	61.8	45.7	37.4	58.8	40.2
c	42.0	62.2	46.0	37.8	59.2	40.8
d	41.0	61.5	44.6	37.1	58.6	40.0

(b) Study on Multi-Level Loss.

Std	AP <sup>bb</sup>	AP <sup>bb</sup> <sub>50</sub>	AP <sup>bb</sup> <sub>75</sub>	AP <sup>mk</sup>	AP <sup>mk</sup> <sub>50</sub>	AP <sup>mk</sup> <sub>75</sub>
None	42.5	62.8	46.9	38.2	59.8	41.2
0.75	42.2	62.3	46.3	37.8	59.4	40.7
0.5	42.0	62.3	45.8	37.8	59.3	40.6

(c) Study on Boundary Smoothness.

Weight Decay	AP <sup>bb</sup>	AP <sup>bb</sup> <sub>50</sub>	AP <sup>bb</sup> <sub>75</sub>	AP <sup>mk</sup>	AP <sup>mk</sup> <sub>50</sub>	AP <sup>mk</sup> <sub>75</sub>
1.5e-6	41.7	62.2	45.9	37.8	59.3	40.6
1.5e-6 Div 1.5	41.8	62.3	45.9	37.8	59.3	40.6
1.5e-6 Div 2	42.2	62.4	46.4	37.8	59.4	40.6
5e-6	42.3	62.6	46.7	38.0	59.7	40.8
1e-5	42.5	62.8	46.9	38.2	59.8	41.2

(d) Study on Weight Decay.

Arch.	AP <sup>bb</sup>	AP <sup>bb</sup> <sub>50</sub>	AP <sup>bb</sup> <sub>75</sub>	AP <sup>mk</sup>	AP <sup>mk</sup> <sub>50</sub>	AP <sup>mk</sup> <sub>75</sub>
B	41.1	61.3	45.4	37.2	58.6	39.9
B+F	41.5	61.6	45.5	37.4	58.6	40.1
B+F+H	42.5	62.8	46.9	38.2	59.8	41.2

(e) Study on Architecture Alignment.

Epoch	AP <sup>bb</sup>	AP <sup>bb</sup> <sub>50</sub>	AP <sup>bb</sup> <sub>75</sub>	AP <sup>bb</sup> <sub>s</sub>	AP <sup>bb</sup> <sub>m</sub>	AP <sup>bb</sup> <sub>l</sub>
100	39.1	58.5	41.8	26.5	43.7	47.3
200	39.5	59.2	42.7	25.8	44.2	47.9
400	39.9	59.8	42.7	26.7	44.4	48.3

(f) Study on Training Epoch.

Table 10: Ablation studies on COCO for the proposed MCL method. All the models are pretrained on ImageNet dataset for 100 epochs and finetuned on COCO dataset following 1x schedule [56]. The loss indicators in (b) are same as those in Fig. 3. None in (c) indicates that the subimages are not smoothed. Div in (d) means all the non-normalization layer parameters are divided by a fixed number. In (e), B means that only the backbone is pre-trained, F indicates FPN neck and H is the detection head. The results are reported with Mask R-CNN in all tables except (f), in which the results of RetinaNet are provided.

which makes output resilient to the parameter scale, we take Batch Normalization [31] for example:  $\text{BN}(Wx) = \text{BN}(\alpha W)x$ , and we can show that:  $\frac{\partial \text{BN}(\alpha Wx)}{\partial \alpha W} = \frac{1}{\alpha} \cdot \frac{\partial \text{BN}(Wx)}{\partial W}$ , where  $\alpha$  is a positive scalar. In the case that  $\alpha < 1$ , the gradient of parameter  $W$  is magnified. Following the SGD update rule, the model weight of  $t+1$  step is  $W_{t+1} = W_t - \eta \frac{1}{\alpha} \frac{\partial \text{BN}(Wx)}{\partial W}$ , where  $\eta$  is the learning rate. Suppose that **the learning rate is suitable** and **the weight is well-initialized**, the relatively small weight norm leads to a faster convergence, compared with the large model weight.

**Architecture Alignment.** We ablate each architecture component step by step to verify the importance of alignment of the downstream and pre-train model architecture. The pre-trained weights of FPN neck and Detection Head are ablated. Tab. 10e reports the studies, in which the baseline achieves 41.1 AP<sup>bb</sup>/37.2 AP<sup>mk</sup>. FPN neck further improves the performance to 41.5 AP<sup>bb</sup>/37.4 AP<sup>mk</sup> and Detection Head finally improves the result to 42.5 AP<sup>bb</sup>/38.2 AP<sup>mk</sup>. Pre-trained Detection Head leads to additional gain for Mask R-CNN, while MCL also outperforms other state-of-the-art methods on the RetinaNet model (as shown in Tab. 2), which has a different detection head and FPN architecture from Mask R-CNN. This phenomenon demonstrates that MCL is somewhat robust to model architecture.

**Training Epochs.** We extend the training epochs to 200 epochs and 400 epochs on the ImageNet. The pre-trained model is finetuned using RetinaNet with the standard 1x COCO schedule. Pre-trained for 200 epochs, MCL improves the detection result to 39.5 AP. Another 200 training epochs increase the performance by 0.4 AP, which means that long training schedule improves the performance.

## 5. Conclusion

In this work, we introduce a novel self-supervised framework based on multi-level contrastive learning. Our method learns regional representation for precise localization, scale consistency among multi-scale crops, and semantic representations that generalize well on the dense prediction tasks. The montage assembly explicitly encodes the absolute position and scale information. Multi-level contrastive learning aligns the feature map with the image region and regularizes the scale consistency. Besides, we empirically explore the alignment between pre-training and finetuning by investigating the transfer performance of applying the proposed pretext task in the supervised learning scenario. Our experiment results demonstrate the state-of-the-art transfer performance on various dense prediction tasks, while significantly reducing the pre-training epochs. A further fine-grain representation learning under our framework may lead to a promising result.

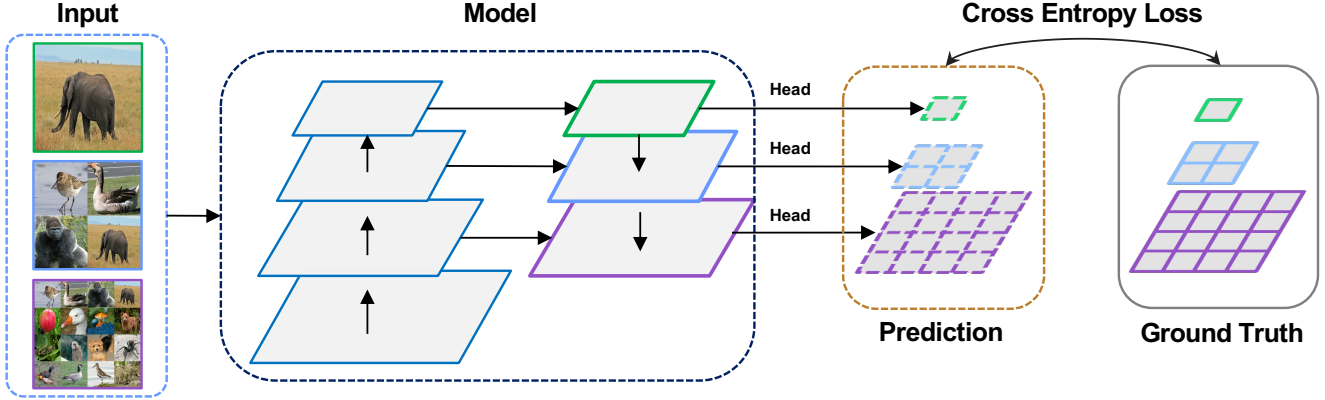


Figure 4: Overview of MCL applied in the supervised scenario. All the input images are augmented via the same pipeline with different seeds. The input images are downsampled and assembled in a montage manner. The ground truths are assembled in the same order as the montage images. The multi-level cross-entropy loss is applied to optimize the model.

## A. Appendix

### A.1. Additional Implementation Details

**Multi-Level Contrastive Loss.** As described in Sec. 3.1, the images are downsampled according to the level index and assembled in a montage manner. The numbers of montage image in level  $i$  is  $\frac{B}{2^i}$ , where  $i$  starts from 0 to  $S-1$  and  $B$  is the batch size. Therefore, the montage assembly increases the computational cost marginally and the upper bounder is twice the baseline batch size. Since the highest resolution images typically yield the best semantic representation and the empirical result in Sec. 4.3, the first level contrastive loss (on the highest resolution images) is important to the representation learning. As a consequence, we assign different loss weight to each level,  $\frac{1}{2^{(i+1)}}$  for the  $i$ -th level. The detection head is a shared 4 CONV head without  $fc$  layer across levels, which are not loaded in the RetinaNet detector. We attach a global average pooling layer on the detection head to aggregate the features because averaging implicitly encourages a high response region. Both the projection head and prediction head are 2-layer MLPs whose hidden layer dimension is 2048. The final linear layer has a 256-dimension output and a final BN layer is attached to the projection head to accelerate the convergence.

**Multi-Level Supervised Learning.** We extend MCL to the supervised learning scenario to demonstrate the importance of the alignment between the pretext task and downstream tasks. As illustrated in Fig. 4, we generate  $S$  augmented views for the model, which are downsampled to  $\frac{1}{2^s}$  original size. We set  $s$  as the level index, which starts from 0 to  $S-1$ . Different from self-supervised learning, we simply adopt the same optimizer as the normal setting, SGD optimizer for ResNet and AdamW optimizer for Swin-Transformer. The other hyperparameters are the same as the baseline counterparts.

## B. Additional Results

**Long Finetuning Schedule.** The experiments in Sec. 4 mainly follow the 1x and 2x schedule, which are not long enough for detectors to be fully converged. We extend the training schedule to 6x schedule, *i.e.* 540k iterations. Tab. 11 shows that MCL pre-trained with 400 epochs achieves 41.2 AP<sup>bb</sup> as 2x schedule is applied. MCL with 6x schedule still surpasses the supervised counterpart and MoCo v2 pre-trained with 800 epochs. These results prove that pre-training not only accelerates the convergence but also improves the final performance.

**Mask R-CNN with C4 on COCO.** As described in Sec. 3.1, MCL is compatible with the non-FPN framework. We construct a feature pyramid by directly interpolating the single-level feature in bilinear mode to the specific sizes. The results in Tab. 12 show that MCL achieves SOTA results while significantly reducing the training epochs. Our method achieves a superior result with a 1x schedule and benefits from a long finetune schedule, *i.e.* 2x COCO schedule. We believe that the reason that MCL yields an inferior result on Mask R-CNN C4, compared with Mask R-CNN FPN, is that Mask R-CNN C4 has only a single-level feature for detection, which yields a lower baseline on the small object detection.

**Linear Evaluation on ImageNet-1K.** MCL learns global semantic representation besides scale consistency and regional localization. We present the ImageNet-1K linear evaluation results for reference. Following the common setting [7, 22, 24], data augmentation contains random crop with resize of  $224 \times 224$  pixels and random flip. Only the backbone network parameters are loaded and frozen. The classification head is trained for 100 epochs, using an SGD optimizer with a momentum of 0.9 and a batch size of 256. The learning rate starts with 10 and the weight decay is 0. In the test phase, the data augmentation is a center

Methods	Epoch	1x schedule			2x schedule			6x schedule		
		AP	AP <sub>50</sub>	AP <sub>75</sub>	AP	AP <sub>50</sub>	AP <sub>75</sub>	AP	AP <sub>50</sub>	AP <sub>75</sub>
Supervised	90	37.4	56.6	39.7	38.8	58.7	41.2	39.2	58.6	42.1
MoCo v2	800	37.9 <sup>(+0.5)</sup>	57.1 <sup>(+0.5)</sup>	40.4 <sup>(+0.7)</sup>	39.8 <sup>(+1.0)</sup>	59.3 <sup>(+0.6)</sup>	42.8 <sup>(+1.6)</sup>	40.2 <sup>(+1.0)</sup>	59.9 <sup>(+1.3)</sup>	43.1 <sup>(+1.0)</sup>
<b>MCL</b>	<b>400</b>	<b>39.9<sup>(+2.5)</sup></b>	<b>59.8<sup>(+3.2)</sup></b>	<b>42.7<sup>(+3.0)</sup></b>	<b>41.2<sup>(+2.4)</sup></b>	<b>61.1<sup>(+2.4)</sup></b>	<b>44.0<sup>(+2.8)</sup></b>	<b>41.4<sup>(+2.2)</sup></b>	<b>61.1<sup>(+2.5)</sup></b>	<b>44.5<sup>(+2.4)</sup></b>

Table 11: Results of the long training schedule for RetinaNet finetuned on COCO with 90k, 180k, and 540k. MCL not only accelerates the convergence but also improves the final performance.

Methods	Epoch	1× Schedule						2× Schedule					
		AP <sup>bb</sup>	AP <sup>bb</sup> <sub>50</sub>	AP <sup>bb</sup> <sub>75</sub>	AP <sup>mk</sup>	AP <sup>mk</sup> <sub>50</sub>	AP <sup>mk</sup> <sub>75</sub>	AP <sup>bb</sup>	AP <sup>bb</sup> <sub>50</sub>	AP <sup>bb</sup> <sub>75</sub>	AP <sup>mk</sup>	AP <sup>mk</sup> <sub>50</sub>	AP <sup>mk</sup> <sub>75</sub>
Rand Init	-	26.4	44.0	27.8	29.3	46.9	30.8	35.6	54.6	38.2	31.4	51.5	33.5
Supervised	90	38.2	58.2	41.2	33.3	54.7	35.2	40.0	59.9	43.1	34.7	56.5	36.9
MoCo [24]	200	38.5	58.3	41.6	33.6	54.8	35.6	40.7	60.5	44.1	35.4	57.3	37.6
SimCLR [10]	200	-	-	-	-	-	-	39.6	59.1	42.9	34.6	55.9	37.1
MoCo v2 [12]	800	39.3	58.9	42.5	34.3	55.7	36.5	41.2	60.9	44.6	35.8	57.7	38.2
InfoMin [48]	200	39.0	58.5	42.0	34.1	55.2	36.3	41.3	61.2	45.0	36.0	57.9	38.3
BYOL [22]	300	-	-	-	-	-	-	40.3	60.5	43.9	35.1	56.8	37.3
SwAV [7]	400	-	-	-	-	-	-	39.6	60.1	42.9	34.7	56.6	36.6
SimSiam [13]	200	39.2	59.3	42.1	34.4	56.0	36.7	-	-	-	-	-	-
PixPro [60]	400	40.5	59.8	44.0	-	-	-	-	-	-	-	-	-
SoCo [54]	100	40.4	60.4	43.7	34.9	56.8	37.0	41.1	61.0	44.4	35.6	57.5	38.0
<b>MCL</b>	<b>100</b>	<b>40.0</b>	<b>60.3</b>	<b>43.2</b>	<b>34.7</b>	<b>56.7</b>	<b>36.7</b>	<b>41.7</b>	<b>61.7</b>	<b>45.4</b>	<b>36.1</b>	<b>58.1</b>	<b>38.5</b>

Table 12: Comparison with SOTA methods on COCO by using Mask R-CNN with R50-C4. All the detectors are evaluated on COCO *val* 2017 set. “-” means that the results are missing in the source paper. MCL achieves SOTA results while significantly reducing the training epochs.

crop from a resized  $256 \times 256$  image. Tab. 13 shows that MCL surpasses SoCo on ImageNet linear evaluation, learning a semantic global representation. Compared with the self-supervised learning methods for image classification, MCL outperforms them on dense prediction tasks, while underperforms some of them on the linear evaluation. This phenomenon shows that the improvement on upstream task does not guarantee a better transfer performance on downstream tasks, due to the task misalignment.

### B.1. Analysis

As discussed in Sec. 1, the scale of objects varies in a small range for ImageNet classification model, whereas the scale deviation of MS-COCO dataset [34] is large across object instances for detectors. As shown in Fig. 5, the standard deviation of the scale of instances in MS-COCO is 188.4, while that of ImageNet is 56.7. Our MCL assembles multi-scale images to augment the scale range and distribution.

Beside, MCL encodes the location of each sub-image explicitly to learn representations for the dense prediction tasks. Fig. 6 shows that MCL performs better than baseline at a high IoU threshold for both RetinaNet and Mask-RCNN detectors, which demonstrates that pre-training is beyond a

strong regularization technique. MCL successfully transfers the strong prior knowledge for precise localization from the pretext task to the downstream tasks.

### References

- [1] NeurIPS 2022. Bridging the gap from asymmetry tricks to decorrelation principles in non-contrastive self-supervised learning. 6
- [2] NeurIPS 2022. Vicregl: Self-supervised learning of local visual features. 6
- [3] ICLR 2023. Designing bert for convolutional networks: Sparse and hierarchical masked modeling. 6
- [4] Pablo Arbeláez, Jordi Pont-Tuset, Jonathan T Barron, Ferran Marques, and Jitendra Malik. Multiscale combinatorial grouping. In *Proceedings of the IEEE conference on computer vision and pattern recognition*, pages 328–335, 2014. 2, 3
- [5] Philip Bachman, R Devon Hjelm, and William Buchwalter. Learning representations by maximizing mutual information across views. *Advances in neural information processing systems*, 32, 2019. 4
- [6] Piotr Bojanowski and Armand Joulin. Unsupervised learning by predicting noise. *arXiv preprint arXiv:1704.05310*, 2017. 2
- [7] Mathilde Caron, Ishan Misra, Julien Mairal, Priya Goyal, Piotr Bojanowski, and Armand Joulin. Unsupervised learning

Methods	100 ep	400 ep
Supervised	76.5	-
SoCo	59.7	62.6
SimCLR	66.5	69.8
MoCo v2	67.4	71.0
SwAV	66.5	70.7
SimSiam	68.1	70.8
<b>MCL</b>	<b>69.9</b>	<b>71.5</b>

Table 13: Comparison with state-of-the-art self-supervised learning methods on ImageNet-1K **linear evaluation** with the ResNet-50 backbone.

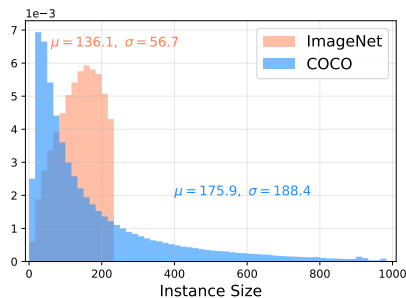


Figure 5: Instance Size Distribution. For the COCO dataset, all the images are resized to (1333, 800) shape. For the ImageNet dataset, all the images are resized to  $224 \times 224$  to calculate the statistics.

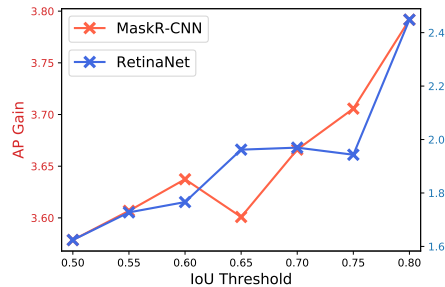


Figure 6: The  $AP^{bb}$  gain of MCL over the supervised counterpart. MCL performs better than the baseline at a higher IoU threshold, indicating that the MCL features have better localization capability.

of visual features by contrasting cluster assignments. *arXiv preprint arXiv:2006.09882*, 2020. [1](#), [2](#), [4](#), [5](#), [6](#), [7](#), [9](#), [10](#)

- [8] Mathilde Caron, Hugo Touvron, Ishan Misra, Hervé Jégou, Julien Mairal, Piotr Bojanowski, and Armand Joulin. Emerging properties in self-supervised vision transformers. In *Proceedings of the International Conference on Computer Vision (ICCV)*, 2021. [6](#)
- [9] Kai Chen, Jiaqi Wang, Jiangmiao Pang, Yuhang Cao, Yu Xiong, Xiaoxiao Li, Shuyang Sun, Wansen Feng, Ziwei Liu, Jiarui Xu, et al. Mmdetection: Open mmlab detection toolbox and benchmark. *arXiv preprint arXiv:1906.07155*, 2019. [7](#)
- [10] Ting Chen, Simon Kornblith, Mohammad Norouzi, and Geoffrey Hinton. A simple framework for contrastive learning of visual representations. In *International conference on machine learning*, pages 1597–1607. PMLR, 2020. [1](#), [2](#), [3](#), [4](#), [7](#), [10](#)
- [11] Ting Chen, Simon Kornblith, Kevin Swersky, Mohammad Norouzi, and Geoffrey E Hinton. Big self-supervised models are strong semi-supervised learners. *Advances in neural information processing systems*, 33:22243–22255, 2020. [2](#)
- [12] Xinlei Chen, Haoqi Fan, Ross Girshick, and Kaiming He. Improved baselines with momentum contrastive learning. *arXiv preprint arXiv:2003.04297*, 2020. [6](#), [10](#)
- [13] Xinlei Chen and Kaiming He. Exploring simple siamese representation learning. In *Proceedings of the IEEE/CVF Conference on Computer Vision and Pattern Recognition*, pages 15750–15758, 2021. [4](#), [10](#)
- [14] Xinlei Chen, Saining Xie, and Kaiming He. An empirical study of training self-supervised vision transformers. In *Proceedings of the IEEE/CVF International Conference on Computer Vision*, pages 9640–9649, 2021. [5](#), [6](#), [7](#)
- [15] Marius Cordts, Mohamed Omran, Sebastian Ramos, Timo Rehfeld, Markus Enzweiler, Rodrigo Benenson, Uwe Franke, Stefan Roth, and Bernt Schiele. The cityscapes dataset for semantic urban scene understanding. In *Proc. of the IEEE Conference on Computer Vision and Pattern Recognition (CVPR)*, 2016. [5](#)
- [16] Jia Deng, Wei Dong, Richard Socher, Li-Jia Li, Kai Li, and Li Fei-Fei. Imagenet: A large-scale hierarchical image database. In *2009 IEEE conference on computer vision and pattern recognition*, pages 248–255. Ieee, 2009. [1](#), [5](#)
- [17] Alexey Dosovitskiy, Lucas Beyer, Alexander Kolesnikov, Dirk Weissenborn, Xiaohua Zhai, Thomas Unterthiner, Mostafa Dehghani, Matthias Minderer, Georg Heigold, Sylvain Gelly, et al. An image is worth 16x16 words: Transformers for image recognition at scale. *arXiv preprint arXiv:2010.11929*, 2020. [7](#)
- [18] Dumitru Erhan, Aaron Courville, Yoshua Bengio, and Pascal Vincent. Why does unsupervised pre-training help deep learning? In *Proceedings of the thirteenth international conference on artificial intelligence and statistics*, pages 201–208. JMLR Workshop and Conference Proceedings, 2010. [1](#)
- [19] Pedro F Felzenszwalb and Daniel P Huttenlocher. Efficient graph-based image segmentation. *International journal of computer vision*, 59(2):167–181, 2004. [3](#)
- [20] Golnaz Ghiasi, Yin Cui, Aravind Srinivas, Rui Qian, Tsung-Yi Lin, Ekin D Cubuk, Quoc V Le, and Barret Zoph. Simple copy-paste is a strong data augmentation method for instance segmentation. In *Proceedings of the IEEE/CVF conference on computer vision and pattern recognition*, pages 2918–2928, 2021. [7](#)
- [21] Ross Girshick. Fast r-cnn. In *Proceedings of the IEEE international conference on computer vision*, pages 1440–1448, 2015. [3](#)
- [22] Jean-Bastien Grill, Florian Strub, Florent Altché, Corentin Tallec, Pierre H Richemond, Elena Buchatskaya, Carl Doersch, Bernardo Avila Pires, Zhaohan Daniel Guo, Mohammad Gheshlaghi Azar, et al. Bootstrap your own latent: A new approach to self-supervised learning. *arXiv preprint arXiv:2006.07733*, 2020. [1](#), [3](#), [4](#), [5](#), [6](#), [7](#), [9](#), [10](#)
- [23] Agrim Gupta, Piotr Dollar, and Ross Girshick. Lvis: A dataset for large vocabulary instance segmentation. In *Proceedings of the IEEE/CVF conference on computer vision and pattern recognition*, pages 5356–5364, 2019. [5](#), [6](#)
- [24] Kaiming He, Haoqi Fan, Yuxin Wu, Saining Xie, and Ross Girshick. Momentum contrast for unsupervised visual representation learning. In *Proceedings of the IEEE/CVF Con-*

- ference on Computer Vision and Pattern Recognition, pages 9729–9738, 2020. 1, 2, 3, 5, 6, 9, 10
- [25] Kaiming He, Ross Girshick, and Piotr Dollár. Rethinking imagenet pre-training. In *Proceedings of the IEEE/CVF International Conference on Computer Vision*, pages 4918–4927, 2019. 1
- [26] Kaiming He, Georgia Gkioxari, Piotr Dollár, and Ross Girshick. Mask r-cnn. In *Proceedings of the IEEE international conference on computer vision*, pages 2961–2969, 2017. 1, 3, 5
- [27] Kaiming He, Xiangyu Zhang, Shaoqing Ren, and Jian Sun. Deep residual learning for image recognition. In *Proceedings of the IEEE conference on computer vision and pattern recognition*, pages 770–778, 2016. 7
- [28] Olivier J Hénaff, Skanda Koppula, Jean-Baptiste Alayrac, Aaron van den Oord, Oriol Vinyals, and João Carreira. Efficient visual pretraining with contrastive detection. In *Proceedings of the IEEE/CVF International Conference on Computer Vision*, pages 10086–10096, 2021. 1, 2, 3, 6
- [29] R Devon Hjelm, Alex Fedorov, Samuel Lavoie-Marchildon, Karan Grewal, Phil Bachman, Adam Trischler, and Yoshua Bengio. Learning deep representations by mutual information estimation and maximization. *arXiv preprint arXiv:1808.06670*, 2018. 4
- [30] Gao Huang, Zhuang Liu, Laurens Van Der Maaten, and Kilian Q Weinberger. Densely connected convolutional networks. In *Proceedings of the IEEE conference on computer vision and pattern recognition*, pages 4700–4708, 2017. 7
- [31] Sergey Ioffe and Christian Szegedy. Batch normalization: Accelerating deep network training by reducing internal covariate shift. In *International conference on machine learning*, pages 448–456. PMLR, 2015. 8
- [32] Zhaowen Li, Yousong Zhu, Fan Yang, Wei Li, Chaoyang Zhao, Yingying Chen, Zhiyang Chen, Jiahao Xie, Liwei Wu, Rui Zhao, et al. Univip: A unified framework for self-supervised visual pre-training. In *Proceedings of the IEEE/CVF Conference on Computer Vision and Pattern Recognition*, pages 14627–14636, 2022. 6
- [33] Tsung-Yi Lin, Priya Goyal, Ross Girshick, Kaiming He, and Piotr Dollár. Focal loss for dense object detection. In *Proceedings of the IEEE international conference on computer vision*, pages 2980–2988, 2017. 1, 5
- [34] Tsung-Yi Lin, Michael Maire, Serge Belongie, James Hays, Pietro Perona, Deva Ramanan, Piotr Dollár, and C Lawrence Zitnick. Microsoft coco: Common objects in context. In *European conference on computer vision*, pages 740–755. Springer, 2014. 5, 10
- [35] Songtao Liu, Zeming Li, and Jian Sun. Self-emd: Self-supervised object detection without imagenet. *arXiv preprint arXiv:2011.13677*, 2020. 1, 3, 5
- [36] Ze Liu, Yutong Lin, Yue Cao, Han Hu, Yixuan Wei, Zheng Zhang, Stephen Lin, and Baining Guo. Swin transformer: Hierarchical vision transformer using shifted windows. In *Proceedings of the IEEE/CVF International Conference on Computer Vision*, pages 10012–10022, 2021. 7
- [37] Ishan Misra and Laurens van der Maaten. Self-supervised learning of pretext-invariant representations. In *Proceedings of the IEEE/CVF Conference on Computer Vision and Pattern Recognition*, pages 6707–6717, 2020. 3, 5
- [38] CVPR 2022 Best paper Finalist. Point-level region contrast for object detection pre-training. 2022. 6
- [39] Pedro O Pinheiro, Amjad Almahairi, Ryan Y Benmalek, Florian Golemo, and Aaron Courville. Unsupervised learning of dense visual representations. *arXiv preprint arXiv:2011.05499*, 2020. 1, 3
- [40] Senthil Purushwalkam and Abhinav Gupta. Demystifying contrastive self-supervised learning: Invariances, augmentations and dataset biases. *Advances in Neural Information Processing Systems*, 33:3407–3418, 2020. 2, 3
- [41] Limeng Qiao, Yuxuan Zhao, Zhiyuan Li, Xi Qiu, Jianan Wu, and Chi Zhang. Defrcn: Decoupled faster r-cnn for few-shot object detection. In *Proceedings of the IEEE/CVF International Conference on Computer Vision*, pages 8681–8690, 2021. 1
- [42] Shaoqing Ren, Kaiming He, Ross Girshick, and Jian Sun. Faster r-cnn: Towards real-time object detection with region proposal networks. *Advances in neural information processing systems*, 28:91–99, 2015. 1
- [43] Byungseok Roh, Wuhyun Shin, Ildoo Kim, and Sungwoong Kim. Spatially consistent representation learning. In *Proceedings of the IEEE/CVF Conference on Computer Vision and Pattern Recognition*, pages 1144–1153, 2021. 6
- [44] Yossi Rubner, Carlo Tomasi, and Leonidas J Guibas. The earth mover’s distance as a metric for image retrieval. *International journal of computer vision*, 40(2):99–121, 2000. 3
- [45] Mark Sandler, Andrew Howard, Menglong Zhu, Andrey Zhmoginov, and Liang-Chieh Chen. Mobilenetv2: Inverted residuals and linear bottlenecks. In *Proceedings of the IEEE conference on computer vision and pattern recognition*, pages 4510–4520, 2018. 7
- [46] Kihyuk Sohn, Zizhao Zhang, Chun-Liang Li, Han Zhang, Chen-Yu Lee, and Tomas Pfister. A simple semi-supervised learning framework for object detection. *arXiv preprint arXiv:2005.04757*, 2020. 1
- [47] Chenxin Tao, Honghui Wang, Xizhou Zhu, Jiahua Dong, Shiji Song, Gao Huang, and Jifeng Dai. Exploring the equivalence of siamese self-supervised learning via a unified gradient framework. In *Proceedings of the IEEE/CVF Conference on Computer Vision and Pattern Recognition*, pages 14431–14440, 2022. 6
- [48] Yonglong Tian, Chen Sun, Ben Poole, Dilip Krishnan, Cordelia Schmid, and Phillip Isola. What makes for good views for contrastive learning? *Advances in Neural Information Processing Systems*, 33:6827–6839, 2020. 5, 6, 10
- [49] Ilya O Tolstikhin, Neil Houlsby, Alexander Kolesnikov, Lucas Beyer, Xiaohua Zhai, Thomas Unterthiner, Jessica Yung, Andreas Steiner, Daniel Keysers, Jakob Uszkoreit, et al. Mlp-mixer: An all-mlp architecture for vision. *Advances in Neural Information Processing Systems*, 34, 2021. 7
- [50] Hugo Touvron, Matthieu Cord, Matthijs Douze, Francisco Massa, Alexandre Sablayrolles, and Hervé Jégou. Training data-efficient image transformers & distillation through attention. In *International Conference on Machine Learning*, pages 10347–10357. PMLR, 2021. 4

- [51] Jasper RR Uijlings, Koen EA Van De Sande, Theo Gevers, and Arnold WM Smeulders. Selective search for object recognition. *International journal of computer vision*, 104(2):154–171, 2013. 2, 3
- [52] Aaron Van den Oord, Yazhe Li, and Oriol Vinyals. Representation learning with contrastive predictive coding. *arXiv e-prints*, pages arXiv–1807, 2018. 4
- [53] Xinlong Wang, Rufeng Zhang, Chunhua Shen, Tao Kong, and Lei Li. Dense contrastive learning for self-supervised visual pre-training. In *Proceedings of the IEEE/CVF Conference on Computer Vision and Pattern Recognition*, pages 3024–3033, 2021. 1, 3, 5, 6
- [54] Fangyun Wei, Yue Gao, Zhirong Wu, Han Hu, and Stephen Lin. Aligning pretraining for detection via object-level contrastive learning. *Advances in Neural Information Processing Systems*, 34, 2021. 1, 2, 3, 5, 10
- [55] Yuxin Wu and Kaiming He. Group normalization. In *Proceedings of the European conference on computer vision (ECCV)*, pages 3–19, 2018. 7
- [56] Yuxin Wu, Alexander Kirillov, Francisco Massa, Wan-Yen Lo, and Ross Girshick. Detectron2. <https://github.com/facebookresearch/detectron2>, 2019. 1, 2, 5, 8
- [57] Zhirong Wu, Yuanjun Xiong, Stella X Yu, and Dahua Lin. Unsupervised feature learning via non-parametric instance discrimination. In *Proceedings of the IEEE Conference on Computer Vision and Pattern Recognition*, pages 3733–3742, 2018. 2, 5
- [58] Tete Xiao, Colorado J Reed, Xiaolong Wang, Kurt Keutzer, and Trevor Darrell. Region similarity representation learning. In *Proceedings of the IEEE/CVF International Conference on Computer Vision*, pages 10539–10548, 2021. 6
- [59] Enze Xie, Jian Ding, Wenhai Wang, Xiaohang Zhan, Hang Xu, Peize Sun, Zhenguo Li, and Ping Luo. Detco: Unsupervised contrastive learning for object detection. In *Proceedings of the IEEE/CVF International Conference on Computer Vision*, pages 8392–8401, 2021. 6
- [60] Zhenda Xie, Yutong Lin, Zheng Zhang, Yue Cao, Stephen Lin, and Han Hu. Propagate yourself: Exploring pixel-level consistency for unsupervised visual representation learning. In *Proceedings of the IEEE/CVF Conference on Computer Vision and Pattern Recognition*, pages 16684–16693, 2021. 1, 3, 5, 6, 10
- [61] Yufei Xu, Qiming Zhang, Jing Zhang, and Dacheng Tao. Regioncl: Exploring contrastive region pairs for self-supervised representation learning. In *European Conference on Computer Vision*, pages 477–494. Springer, 2022. 6
- [62] Ceyuan Yang, Zhirong Wu, Bolei Zhou, and Stephen Lin. Instance localization for self-supervised detection pretraining. In *Proceedings of the IEEE/CVF Conference on Computer Vision and Pattern Recognition*, pages 3987–3996, 2021. 1, 5, 6
- [63] Mang Ye, Xu Zhang, Pong C Yuen, and Shih-Fu Chang. Unsupervised embedding learning via invariant and spreading instance feature. In *Proceedings of the IEEE/CVF Conference on Computer Vision and Pattern Recognition*, pages 6210–6219, 2019. 4
- [64] Yang You, Igor Gitman, and Boris Ginsburg. Large batch training of convolutional networks. *arXiv preprint arXiv:1708.03888*, 2017. 5
- [65] Cheng Zhang, Tai-Yu Pan, Yandong Li, Hexiang Hu, Dong Xuan, Soravit Changpinyo, Boqing Gong, and Wei-Lun Chao. Mosaicos: a simple and effective use of object-centric images for long-tailed object detection. In *Proceedings of the IEEE/CVF International Conference on Computer Vision*, pages 417–427, 2021. 7